COMMUNICATION

Check for updates

Increased thermal stability and retained antibacterial properties in a sulbactam and amantadine salt: towards effective antibacterial–antiviral combination therapies†
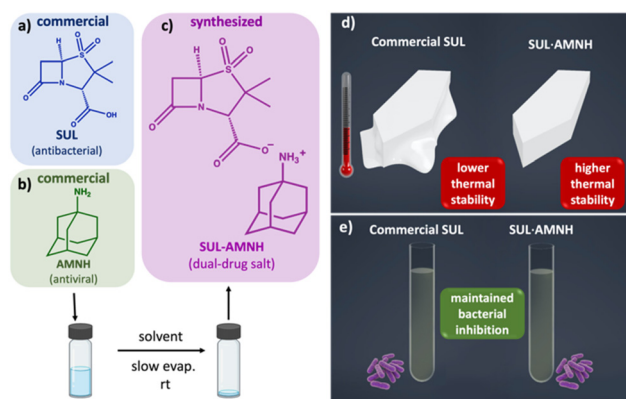
Josephine Bicknell, [ID] [a] Ivan Bondarenko, [ID] [a] Alice Colatrella, [ID] [a]
Elani J. Cabrera-Vega, [ID] [b] Jesus Daniel Loya, [ID] [a] Delbert S. Botes, [ID] [c]
Jay L. Mellies [ID] *[d] and Gonzalo Campillo-Alvarado [ID] *[a]

We describe the formation of a multidrug salt comprising sulbactam (SUL, β-lactamase inhibitor) and amantadine (AMNH, antiviral). Physicochemical investigation of the SUL·AMNH salt revealed enhanced thermal stability compared to pristine starting materials. *In vitro* studies found that salt formation in SUL·AMNH does not disrupt antibacterial activity against model organisms *Escherichia coli* and *Staphylococcus epidermidis*. To our knowledge, we show the first β-lactamase inhibitor-antiviral salt where both components have been approved by the U.S. Food and Drug Administration (FDA), and the first multicomponent solid containing SUL. We envisage our strategy could inspire the design of multicomponent solids for antimicrobial combination therapies.

The World Health Organization (WHO) and the U.S. Centers for Disease Control and Prevention (CDC) warn that without the rapid development of new antimicrobial formulations, treatments for bacterial infections will become obsolete due to antimicrobial resistance (AMR).[1–3] Bacterial–viral coinfections are an important contributor to the anticipated medical and economic burden of AMR.[4] Gaining widened attention during the COVID-19 pandemic, bacterial–viral coinfections impacted nearly 10% of all critically ill COVID-19 patients, such that patients would receive antibiotic regimens in addition to available antiviral medications.[5] The reduced efficacy of single-drug therapies and exacerbation of antimicrobial comorbidities demand immediate dual-pharmaceutical strategies to alleviate the toll of AMR.[6]

[a]Department of Chemistry, Reed College, Portland, OR 97202, USA.
E-mail: gcampillo@reed.edu; Tel: +1 (503) 517 7469
[b]Department of Chemistry, Portland State University, OR 97201, USA
[c]Department of Chemistry, University of Missouri, Columbia, MO 65211, USA
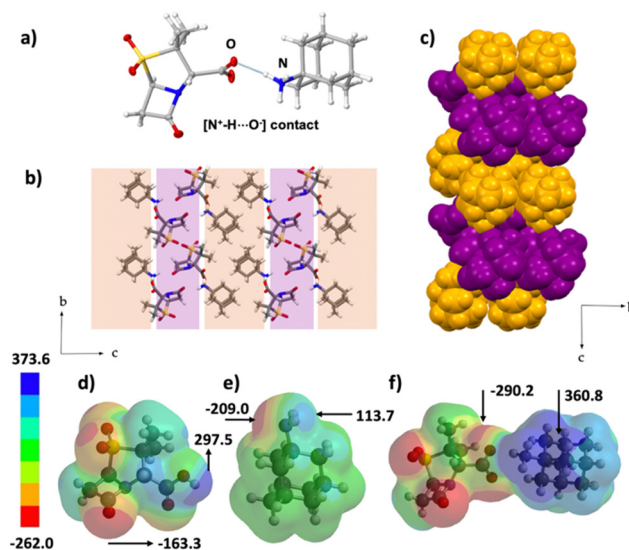[d]Department of Biology, Reed College, Portland, OR 97202, USA

An emerging route for pharmaceutical innovation is pharmaceutical drug–drug cocrystallization (*e.g.*, Entresto, Seglentis) or salt formation (*i.e.*, multicomponent solids).[7–10] In the past five years, multicomponent solids with antibiotics have demonstrated marked improvement in the antibacterial activity of antimicrobial compounds.[11–13] Inspired by these recent advances, we asked whether forming a multicomponent salt with sulbactam would retain its antibacterial properties. This study presents a dual-drug salt comprising antibacterial sulbactam (**SUL**) and antiviral amantadine (**AMNH**) (Scheme 1).

The multicomponent solid **SUL·AMNH** shows sustained antibacterial activity and improved thermal stabilities compared to pristine **SUL**. **SUL** is an antibacterial compound and irreversible β-lactamase inhibitor (BLI) that prevents β-lactamase-positive bacteria from hydrolyzing β-lactam antibiotics.[14] Because **SUL** targets resistance mechanisms rather than acting with explicit bactericidal effect, in clinical practice,

Scheme 1 Physicochemical and pharmaceutical properties of antibacterial–antiviral salt, **SUL·AMNH**: (a–c) molecular structures of **SUL** and **AMNH** and their resulting ionized multicomponent solid, **SUL·AMNH**. (d and e) Enhanced thermal stability and maintained bacterial inhibition of **SUL·AMNH**.

it is typically administered in a 1 : 2 with a primary β-lactam antibiotic, such as Ampicillin. **AMNH** is an antiviral used for treating influenza A subtypes that has also demonstrated *in vitro* inhibition of SARS-CoV-2.[15] Given that both **SUL** and **AMNH** are seminal active pharmaceutical ingredients (APIs) approved by the U.S. Food and Drug Administration (FDA), this work explores the **SUL·AMNH** salt as an initial approach toward developing effective combination therapies against bacterial–viral coinfections.[16,17] As the first dual-drug solid with **SUL** and the first BLI-antiviral salt, our work further demonstrates how solid-state engineering can integrate current FDA-approved BLIs, creating novel BLI-antiviral multicomponent solids that retain antimicrobial properties upon salt formation.

Our design strategy involved the selection of **SUL** (BLI) as a hydrogen bond donor and **AMNH** (antiviral) as a hydrogen bond acceptor. Similar strategies have been employed to synthesize pharmaceutical salts and cocrystals of norfloxacin-sulfathiazole and resveratrol-amantadine hydrochloride.[18,19] Here, powders of **SUL** (25.0 mg, 0.107 mmol) and **AMNH** (16.2 mg, 0.107 mmol) were combined using liquid-assisted grinding (LAG, 3 drops methanol) in a mechanochemical ball mill (Retsch 400 MM, 1 stainless steel ball, 7 mm, 10 ml stainless steel jar) for 30 minutes. The resulting solid was examined by powder X-ray diffraction (PXRD), which revealed the formation of a new phase (Fig. S1, ESI†). The ground solids were dissolved and sonicated in methanol (2 mL), and the solution was incubated at room temperature. White, needle-like single crystals formed after five days of slow evaporation. The composition of **SUL·AMNH** single crystals was determined to be a 1 : 1 ratio of the pharmaceutical components by ^{1}H NMR spectroscopy (Fig. S2, ESI†).

Single crystal X-ray diffraction (SCXRD) confirmed the formation of a multicomponent salt between **SUL** and **AMNH**. Specifically, the components in **SUL·AMNH** crystallize in the monoclinic space group $P2_1$ to form a two-component drug–drug ionic assembly (1 : 1 ratio) sustained by $[N^+–H\cdots O^-]$ ionic interactions (dD···A = 2.743 Å) (Fig. 1a).[20,21] The pK_a rule supported the favorability of the ionized complexes (see ESI† for calculation).[22] The β-lactam ketone exhibits hydrogen bonding (dN–H···O = 2.879 Å) with the ammonium hydrogen, orienting **AMNH** molecules to form a lipophilic aggregate with adamantyl motifs (Fig. 1b).[23] Additional evidence for the formation of the drug–drug salt was provided by Fourier transform infrared (FT-IR) spectroscopy, which showed the formation of the carboxylate anion and ammonium cation (Fig. S3, ESI†). The adamantyl groups in **AMNH** aggregate in an interlocking pattern, creating a tightly organized hydrophobic layer in the *bc*-plane (Fig. 1c). The hydrophilic regions occupied by **SUL** molecules are supported by weak hydrogen bonds between sulbactam's β-lactam hydrogen and deprotonated carboxylic acid [dC–H···O = 3.233 Å]. The simulated PXRD pattern from the crystal structure of **SUL·AMNH** matches the experimental pattern from mechanochemical experiments.
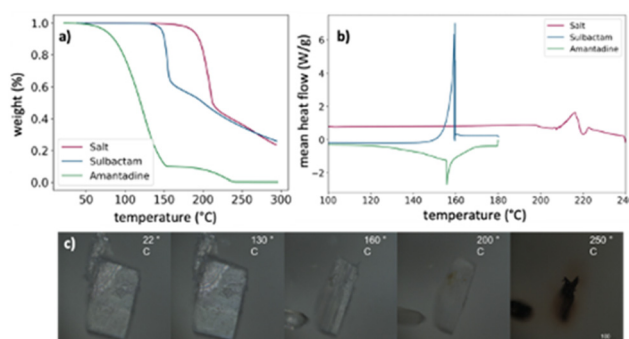
The electronic properties of antibacterial–antiviral salt were rationalized by density functional theory (DFT) electrostatic

Fig. 1 X-ray crystal structure and molecular modelling of **SUL·AMNH**: (a) molecular units sustained by $[N^+–H\cdots O^-]$ ionic interactions, (b) lipophilic assemblies of salt aggregates in the *bc*-plane, (c) space-fill view of level sheets along the *b*-axis, (d–f) density functional theory calculations for starting materials and resulting drug–drug salt. Scale bar and values in kJ mol^{-1}.

potential calculations (ωB97X-D/cc-pVTZ basis set) based on molecular coordinates from SCXRD analysis. Analysis of **SUL** highlighted the Lewis acidity of the carboxylic acid with a positive band of 303.9 kJ mol^{-1} (Fig. 1d). The **AMNH** interactive counterpart, the primary amine, showed high electron-donating capacity at 192.8 kJ mol^{-1} (Fig. 1e). The resulting proton transfer yields strong polarity in the **SUL·AMNH** electron density, with **SUL** carboxylate at 262.0 kJ mol^{-1} and **AMNH** ammonium cation at 373.6 kJ mol^{-1} (Fig. 1f).

The solid of **SUL·AMNH** showed increased thermal stability, as observed by thermogravimetric analysis (TGA), differential scanning calorimetry (DSC) analyses, and hot-stage polarized optical microscopy (POM) (Fig. 2). For **SUL·AMNH**, TGA showed a decomposition point onset at *ca.* 178 °C, which was associated by the observation of an exotherm followed by an

Fig. 2 Thermal properties of **SUL·AMNH** solid. (a) TGA and (b) DSC traces of **SUL·AMNH**, **SUL**, and **AMNH**. (c) Hot-stage POM of a single crystal of **SUL·AMNH**.

endotherm in the DSC trace. **SUL** and **AMNH** showed decomposition onsets at *ca.* 137 °C and 61.3 °C, respectively. Notably, the results demonstrated increased thermal stability of **SUL·AMNH** in the solid state compared to the pristine starting materials (**SUL** and **AMNH**), suggesting the formation of stronger intermolecular forces (Fig. 2a and b).[24] The increase in thermal stability observed in **SUL·AMNH** *via* salt formation is comparable to that of commercial salts, amantadine hydrochloride and sulbactam sodium (Fig. S4–S13†), though moderately lower. Hot-stage POM showed a **SUL·AMNH** crystal to maintain structural integrity up to 160 °C, exhibiting a disintegrative fracture after this point. The disintegrated crystal melts at *ca.* 200 °C followed by decomposition into a dark solid (Fig. 2c).

The favorable intermolecular interactions in **SUL·AMNH** were further evidenced with ^{1}H NMR spectroscopy studies, which showed protons in **SUL·AMNH** to have distinct chemical shifts compared to pristine components (Fig. S2, ESI†) due to protonation.[25,26] Dynamic light scattering (DLS) confirmed the formation of larger aggregates (average particle diameter of
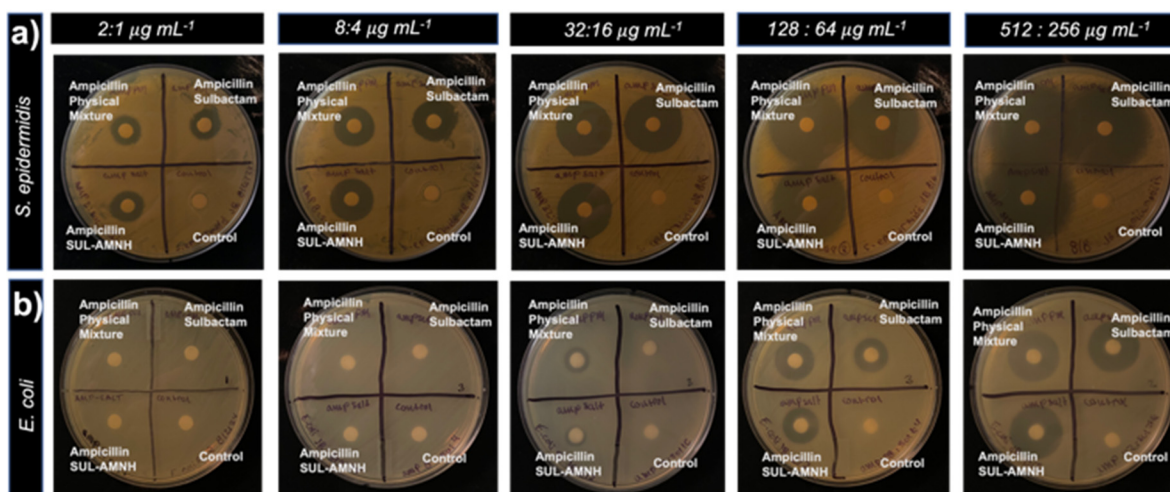
4.86 μm ± 0.71 μm) in solution (50 mg in 3 mL of water) compared to individual components, which showed average diameters of 2.81 μm ± 0.61 μm, and 2.37 μm ± 0.65 μm for **SUL** and **AMNH**, respectively. The observations prompted us to evaluate the applicability of the **SUL·AMNH** solid aggregate in biological assays to assess antimicrobial activity.

The **SUL·AMNH** dual-drug salt showed antibacterial effect of **SUL** in standard clinical 2:1 combination with β-lactam antibiotic ampicillin (**AMP**) (Table 1). The synergistic effect of combined **SUL-AMP** treatment is well established, with the bactericidal activity of AMP bolstered by the innate antibacterial and β-lactamase inhibition activity of **SUL**. Zone of inhibition analysis performed through disk diffusion evaluated the bacterial inhibition of **SUL·AMNH**, pristine **SUL**, and **PM** against *Escherichia coli* and *Staphylococcus epidermidis* at five Clinical & Laboratory Standards Institute (CLSI) and European Committee on Antimicrobial Susceptibility Testing (EUCAST) recommended concentration breakpoints (Table 1).[27] Fresh and actively dividing *E. coli* and *S. epidermidis* microbial cultures (1.5×10^8 CFU mL^{-1}) were plated on Mueller Hinton agar

Table 1 Diameter values of bacterial zones of inhibition for **AMP-SUL·AMNH**, **AMP-SUL**, and **AMP-PM** (mm, Mean $\pm$ SD, n = 3)

Diameter (mm)						
	E. coli			*S. epidermidis*		
		Physical			Physical	
				SUL[a]		Mixture[a]
[C] (μg mL^{-1})	**SUL**[a]	Mixture[a]	**SUL·AMNH**[a]	**SUL·AMNH**[a]		
2:1	0	0	0	10.45 ± 3.1	15.3 ± 1.3	15.8 ± 1.3
8:4	0	0	0	23.0 ± 3.3	22.9 ± 3.1	22.7 ± 3.2
32:16	9.0 ± 0.9	11.4 ± 0.9	10.1 ± 0.6	29.4 ± 2.0	29.8 ± 3.1	29.2 ± 2.1
128:64	17.7 ± 0.7	19.6 ± 0.2	18.7 ± 0.4	41.7 ± 3.2	42.5 ± 4.6	41.6 ± 4.5
512:256	24.6 ± 4	25.0 ± 0.7	24.4 ± 0.2	48.6 ± 1.2	49.8 ± 0.4	50.6 ± 2.4

[a] SUL, physical mixture, and **SUL·AMNH** treatments were each tested in 1:2 ratio with antibiotic Ampicillin.

Fig. 3 Bacterial zones of inhibition at five concentrations of **AMP-SUL·AMNH**, **AMP-SUL**, **AMP-PM**, and Milli-Q water-sodium phosphate buffer (blank) against *S. epidermidis* (a) and *E. coli* (b).

via a non-toxic sterile swab. Sterile paper disks (7 mm) were impregnated with the antibacterial components, placed on the plates, and incubated for 24 h at 37 °C. Correlated CLSI inhibition standards and ANOVA analysis found that *E. coli* showed statistically equivalent resistance against **AMP-SUL**, **AMP-PM**, and **AMP-SUL·AMNH** at lower tested concentrations (2 : 1 µg mL^{-1} and 8 : 4 µg mL^{-1}).[28] At higher tested concentrations (32 : 16 µg mL^{-1}, 128 : 64 µg mL^{-1}, 512 : 256 µg mL^{-1}), increased zones of inhibition presented marked antibacterial sensitivity (Fig. 3). This trend is in agreement with established susceptibility concentrations of BSL-1 *E. coli* for ampicillin-sulbactam treatment.[29] Susceptibility of *S. epidermidis* found similar statistical equivalence in **AMP-SUL**, **AMP-PM**, and **AMP-SUL·AMNH** antibacterial activity. As predicted by CLSI values, *S. epidermidis* showed resistance at 2 : 1 µg mL^{-1} and intermediate susceptibility 8 : 4 µg mL^{-1} concentrations.[28] At the mid-concentration breakpoint of 32 : 16 µg mL^{-1}, increasing zones of bacterial inhibition corresponded to increased sensitivity that became high sensitivity for the remaining tested concentrations (128 : 64 µg mL^{-1} and 512 : 256 µg mL^{-1}). These findings were corroborated with additional investigations of growth analysis by broth microdilution (5 × 10^5 CFU mL^{-1}), which found enhanced and immediate inhibition at even the lowest concentrations over a 14 h period of monitored growth (Fig. S17, ESI†).[27,29] The retention of antibacterial susceptibility among **SUL**, **PM**, and **SUL·AMNH** alongside **AMP** demonstrates that the addition of API **AMNH** does not disrupt the antibacterial activity in **SUL·AMNH** and performs as effectively as pristine **SUL**.

Conclusions

In summary, we successfully synthesized the multicomponent solid **SUL·AMNH** comprising BLI and antiviral APIs. To our knowledge, **SUL·AMNH** is the first BLI-antiviral salt, and multicomponent solid to feature **SUL**, where both APIs are FDA-approved. **SUL·AMNH** showed improved thermal stability compared to pristine **SUL** and **AMNH**, and showed antibacterial properties against *Escherichia coli* and *Staphylococcus epidermidis*. The addition of **AMNH** did not compromise the antibacterial activity despite the strong interaction observed in ^{1}H NMR and DFT calculations. We envisage the design strategy involving multidrug solids (*e.g.*, antibacterial–antiviral) could accelerate the approval of effective pharmaceutical formulations for co-infections (*e.g.*, viral, bacteria) and combination therapies.

Author contributions

J. B. carried out investigation, methodology, data curation, validation, writing and reviewing the original draft. I. B., A. C., E. J. C.-V., J. D. L., D. S. B., carried out formal analysis, data curation, investigation and visualization. J. L. M. and G. C.-A. carried out conceptualization, funding acquisition, formal analysis, project administration, writing, and reviewing the original draft.

Data availability

The authors confirm that the data supporting the findings of this study are available within the article [and/or] its ESI.†

Conflicts of interest

There are no conflicts to declare.

Acknowledgements

References

1 D. G. J. Larsson and C.-F. Flach, Antibiotic Resistance in the Environment, *Nat. Rev. Microbiol.*, 2022, **20**(5), 257–269, DOI: **10.1038/s41579-021-00649-x.**

2 World Health Organization, *Antimicrobial Resistance: Global Report on Surveillance*, World Health Organization, Geneva, 2014.

3 Centers for Disease Control and Prevention (U.S.), *Antibiotic Resistance Threats in the United States, 2019*, Centers for Disease Control and Prevention (U.S.), 2019. DOI: **10.15620/cdc:82532.**

4 T. M. Rawson, D. Ming, R. Ahmad, L. S. P. Moore and A. H. Holmes, Antimicrobial Use, Drug-Resistant Infections and COVID-19, *Nat. Rev. Microbiol.*, 2020, **18**(8), 409–410, DOI: **10.1038/s41579-020-0395-y.**

5 J. Oliva and O. Terrier, Viral and Bacterial Co-Infections in the Lungs: Dangerous Liaisons, *Viruses*, 2021, **13**(9), 1725, DOI: **10.3390/v13091725.**

6 M. Baym, L. K. Stone and R. Kishony, Multidrug Evolutionary Strategies to Reverse Antibiotic Resistance, *Science*, 2016, **351**(6268), aad3292, DOI: **10.1126/science.aad3292.**

7   M. Bashimam and H. El-Zein, Pharmaceutical Cocrystal of Antibiotic Drugs: A Comprehensive Review, *Heliyon*, 2022, **8**(12), e11872, DOI: **10.1016/j.heliyon.2022.e11872**.

8   G. Campillo-Alvarado, E. A. Keene, D. C. Swenson and L. R. MacGillivray, Repurposing of the Anti-HIV Drug Emtricitabine as a Hydrogen-Bonded Cleft for Bipyridines *via* Cocrystallization, *CrystEngComm*, 2020, **22**(21), 3563–3566, DOI: **10.1039/D0CE00474J**.

9   G. Campillo-Alvarado, C. A. Staudt, M. J. Bak and L. R. MacGillivray, Generation of Cocrystals of Tavaborole (AN2690): Opportunities for Boron-Containing APIs, *CrystEngComm*, 2017, **19**(22), 2983–2986, DOI: **10.1039/C7CE00314E**.

10 G. Campillo-Alvarado, T. D. Didden, S. M. Oburn, D. C. Swenson and L. R. MacGillivray, Exploration of Solid Forms of Crisaborole: Crystal Engineering Identifies Polymorphism in Commercial Sources and Facilitates Cocrystal Formation, *Cryst. Growth Des.*, 2018, **18**(8), 4416–4419, DOI: **10.1021/acs.cgd.8b00375**.

11 A. Bonetti, B. Tugnoli, A. Piva and E. Grilli, Thymol as an Adjuvant to Restore Antibiotic Efficacy and Reduce Antimicrobial Resistance and Virulence Gene Expression in Enterotoxigenic Escherichia Coli Strains, *Antibiotics*, 2022, **11**(8), 1073, DOI: **10.3390/antibiotics11081073**.

12 X.-N. Hua, X. Pan, Y. Zhu, Z. Cai, Q. Song, Y. Li, W. Feng, X. Chen, H. Zhang and B. Sun, Novel Pharmaceutical Salts of Cephalexin with Organic Counterions: Structural Analysis and Properties, *RSC Adv.*, 2022, **12**(54), 34843–34850, DOI: **10.1039/D2RA05565A**.

13 L.-Y. Wang, F.-Z. Bu, Y.-T. Li, Z.-Y. Wu and C.-W. Yan, A Sulfathiazole–Amantadine Hydrochloride Cocrystal: The First Codrug Simultaneously Comprising Antiviral and Antibacterial Components, *Cryst. Growth Des.*, 2020, **20**(5), 3236–3246, DOI: **10.1021/acs.cgd.0c00075**.

14 D. Carcione, C. Siracusa, A. Sulejmani, V. Leoni and J. Intra, Old and New Beta-Lactamase Inhibitors: Molecular Structure, Mechanism of Action, and Clinical Use, *Antibiotics*, 2021, **10**(8), 995, DOI: **10.3390/antibiotics10080995**.

15 K. Fink, A. Nitsche, M. Neumann, M. Grossegesse, K.-H. Eisele and W. Danysz, Amantadine Inhibits SARS-CoV-2 In Vitro, *Viruses*, 2021, **13**(4), 539, DOI: **10.3390/v13040539**.

16 D. Wong and D. Van Duin, Novel Beta-Lactamase Inhibitors: Unlocking Their Potential in Therapy, *Drugs*, 2017, **77**(6), 615–628, DOI: **10.1007/s40265-017-0725-1**.

17 E. De Clercq, Antiviral Agents Active against Influenza A Viruses, *Nat. Rev. Drug Discovery*, 2006, **5**(12), 1015–1025, DOI: **10.1038/nrd2175**.

18 S. P. Gopi, S. Ganguly and G. R. Desiraju, A Drug–Drug Salt Hydrate of Norfloxacin and Sulfathiazole: Enhancement of *in Vitro* Biological Properties via Improved Physicochemical Properties, *Mol. Pharm.*, 2016, **13**(10), 3590–3594, DOI: **10.1021/acs.molpharmaceut.6b00320**.

19 L.-Y. Wang, M.-Y. Zhao, F.-Z. Bu, Y.-Y. Niu, Y.-M. Yu, Y.-T. Li, C.-W. Yan and Z.-Y. Wu, Cocrystallization of Amantadine Hydrochloride with Resveratrol: The First Drug–Nutraceutical Cocrystal Displaying Synergistic Antiviral Activity, *Cryst. Growth Des.*, 2021, **21**(5), 2763–2776, DOI: **10.1021/acs.cgd.0c01673**.

20 A. Gunnam, K. Suresh and A. Nangia, Salts and Salt Cocrystals of the Antibacterial Drug Pefloxacin, *Cryst. Growth Des.*, 2018, **18**(5), 2824–2835, DOI: **10.1021/acs.cgd.7b01600**.

21 P. P. Bag, S. Ghosh, H. Khan, R. Devarapalli and C. Malla Reddy, Drug–Drug Salt Forms of Ciprofloxacin with Diflunisal and Indoprofen, *CrystEngComm*, 2014, **16**(32), 7393–7396, DOI: **10.1039/C4CE00631C**.

22 A. J. Cruz-Cabeza, Acid–Base Crystalline Complexes and the pKa Rule, *CrystEngComm*, 2012, **14**(20), 6362, DOI: **10.1039/c2ce26055g**.

23 J. Bicknell, S. A. Agarwal, K. J. Petersen, J. D. Loya, N. Lutz, P. M. Sittinger, S. J. Teat, N. S. Settineri and G. Campillo-Alvarado, Engineering Lipophilic Aggregation of Adapalene and Adamantane-Based Cocrystals via van Der Waals Forces and Hydrogen Bonding, *Cryst. Growth Des.*, 2024, **24**(12), 5222–5230, DOI: **10.1021/acs.cgd.4c00457**.

24 S. Aitipamula, A. B. H. Wong, P. S. Chow and R. B. H. Tan, Novel Solid Forms of Oxaprozin: Cocrystals and an Extended Release Drug–Drug Salt of Salbutamol, *RSC Adv.*, 2016, **6**(41), 34110–34119, DOI: **10.1039/C6RA01802E**.

25 I. Wawer, M. Pisklak and Z. Chilmonczyk, 1H, 13C, 15N NMR Analysis of Sildenafil Base and Citrate (Viagra) in Solution, Solid State and Pharmaceutical Dosage Forms, *J. Pharm. Biomed. Anal.*, 2005, **38**(5), 865–870, DOI: **10.1016/j.jpba.2005.01.046**.

26 H. Kim, C. R. Babu and D. J. Burgess, Quantification of Protonation in Organic Solvents Using Solution NMR Spectroscopy: Implication in Salt Formation, *Int. J. Pharm.*, 2013, **448**(1), 123–131, DOI: **10.1016/j.ijpharm.2013.03.040**.

27 I. Wiegand, K. Hilpert and R. E. W. Hancock, Agar and Broth Dilution Methods to Determine the Minimal Inhibitory Concentration (MIC) of Antimicrobial Substances, *Nat. Protoc.*, 2008, **3**(2), 163–175, DOI: **10.1038/nprot.2007.521**.

28 CLSI, *Performance Standards for Antimicrobial Susceptibility Testing*, 30th edn, CSI supplement M100, Clinical and Laboratory Standards Institute, Wayne, PA, 2020.

29 K. C. Lamp and M. K. Vickers, Pharmacodynamics of Ampicillin-Sulbactam in an In Vitro Infection Model against *Escherichia Coli* Strains with Various Levels of Resistance, *Antimicrob. Agents Chemother.*, 1998, **42**(2), 231–235, DOI: **10.1128/AAC.42.2.231**.